Available online at www.sciencedirect.com
ScienceDirect
Materials Chemistry and Physics 101 (2007) 63–68
MATERIALS CHEMISTRY AND PHYSICS
www.elsevier.com/locate/matchemphys

Cycling performance of $Li[Li_{2/10}Ni_{1/10}Co_{2/10}Mn_{5/10}]O_2$ synthesized by sol–gel route

Chi Hoon Song [a], A. Manuel Stephan [a,1], Yoon Sung Lee [b], Kee Suk Nahm [a,*]

[a] *School of Chemical Engineering and Technology, Chonbuk National University, Chonju 561-756, South Korea*
[b] *Faculty of Applied Chemical Engineering, Chonnam University, Kwangju 500-757, South Korea*

Received 17 January 2006; received in revised form 6 February 2006; accepted 14 February 2006

Abstract

$Li[Li_{2/10}Ni_{1/10}Co_{2/10}Mn_{5/10}]O_2$ was synthesized by a sol–gel method using glycolic acid as chelating agent. The prepared compound was subjected to XRD, SEM, cyclic voltammetry and charge–discharge analysis. The electrochemical studies reveal that the compound, $Li[Li_{2/10}Ni_{1/10}Co_{2/10}Mn_{5/10}]O_2$, delivers a capacity of about 340 mAh g^{-1} during the first charging cycle with an irreversible capacity loss of 180 mAh g^{-1} and also undergoes capacity fading upon prolonged cycling. The cyclic voltammetry data are reflected in the charge–discharge studies. The effect of the dopants on the electrochemical properties of the compound is discussed.

Keywords: Lithium battery; Sol–gel route; Cyclic voltammetry; Charge–discharge characteristics

1. Introduction

The development of lithium batteries has gained an unprecedented significance in the last two decades, as the demand for portable telecommunication devices, computers and eventually hybrid electric vehicles has been on the rise [1–3]. Among the lithium transition-metal oxides studied so far as possible cathode materials for lithium batteries, layered $LiMeO_2$ (Me = 3d transition-metal element) with a α-$NaFeO_2$ structure has drawn the attention of many researchers [4]. Although the commercialized lithium batteries with $LiCoO_2$ possess good reversibility and rate capability, their high cost and toxicity still remain a problem area [5,6]. On the other hand $LiNiO_2$ based cells render electrolytes less prone to oxidation and also leads to poor stoichiometry [7]. In the recent past, several reports are available on cathodes based on $LiMn_2O_4$, which offers a theoretical capacity of 148 mAh g^{-1}, excellent reversibility for the lithium intercalation reaction, good voltage regulation on cycling especially in the 4 V region at ambient temperature, and are inexpensive and eco-friendly [8–10]. However, it exhibits a significant capacity loss when cycled in the 3 V region. On the other hand, $LiMnO_2$ exhibits better cycling performance than $LiMn_2O_4$ spinel when cycled between 2 and 4.5 V versus Li [11–16]. The charge–discharge rate capability, the electrode formulation and the safety of the cells are mainly influenced by the particle size and the morphology of the cathode materials and high current densities could be realized by improved mass transport arising out of much reduced distance in nanoparticle-based systems [17,18]. Furthermore, the lattice parameters of the smaller particles are not much affected when compared with larger one. The conventionally prepared cathode materials using solid-state method requires long calcination time with intermittent grinding and moreover this method has several disadvantages like inhomogeneity, irregular morphology, larger particle size and poor stoichiometry. On the other hand, the preparation of cathode materials by sol–gel method has several advantages like smaller particles of uniform size, better stoichiometry and relatively low calcination temperature [19–22]. As we discussed in our earlier report [23], the structural and electrochemical properties of Li-ion in layered manganese oxide solid solutions vary greatly when they are doped in the transition metal layers. In order to find this a systematic study is obviously required and this study focuses the redox process of $Li[Li_{2/10}Ni_{1/10}Co_{2/10}Mn_{5/10}]O_2$ material at different voltage regions namely, 2.5–4.1, 2.5–4.3, 2.5–4.5, 2.5–4.6 and 2.5–4.8 V, respectively. The compound, $Li[Li_{2/10}Ni_{1/10}Co_{2/10}Mn_{5/10}]O_2$ was prepared by sol–gel

* Corresponding author. Tel.: +82 63 270 2311; fax: +82 63 270 2306.
E-mail address: nahmks@chonbuk.ac.kr (K.S. Nahm).
[1] On deputation from Central Electrochemical Research Institute, Karaikudi 630006, India.

0254-0584/$ – see front matter © 2006 Elsevier B.V. All rights reserved.
doi:10.1016/j.matchemphys.2006.02.015

method using glycolic acid as chelating agent and the structural and electrochemical features of the product as lithium-intercalating cathode materials are presented.

2. Experimental

Stoichiometric amounts of CH_3COO $Li{\cdot}2H_2O$ $(CH_3COO)_2Ni{\cdot}4H_2O$ $(CH_3COO)_2$ $Mn{\cdot}4H_2O$, $(CH_3COO)_2$ $Co{\cdot}4H_2O$ were dissolved in double distilled water. The glycolic acid was used as chelating agent and the pH of the solution was maintained between 5 and 5.5 using nitric acid. The prepared solution was evaporated between 70 and 80 °C. The resulting precursors were decomposed at 450 °C with a ramping rate of 1 °C min^{-1} for 10 h in air. Thus, the decomposed powders were calcined for 10 h at 950 °C with intermittent grinding.

The powder X-ray diffraction (XRD, D/Max 2500, Rigaku) measurement using Cu Kα radiation was employed to characterize the crystalline phase of the synthesized material. The morphology of prepared material was observed by field emission scanning electron microscope (FE-SEM, S-4700, Hitach). The electrochemical characterization was carried out using 2032-type coin cell (Hohsen). For the fabrication of cathode electrode, 20 mg of prepared compounds were mixed with 12 mg of conductive binder (8 mg of Teflonized acetylene black and 4 mg of graphite). The mixture was pressed on 20 mm^2 stainless steel mesh used as the current collector and dried at 100 °C for 10 h in a vacuum oven. The cells were composed of the cathode and the lithium foil (Cyprus Foote Mineral) anode, separated by porous polypropylene film separator (Celgard 3401). The electrolyte was a 1 M $LiPF_6$-ethylene carbonate (EC)/dimethyl carbonate (DMC) with a 1:2 volume ratio (E. Merck). The cells were assembled in an argon-filled dry box and tested at room temperature. All cells were charged and discharged at a current density of 0.4 mA cm^{-2} with a voltage range between 2.5 and 4.8 V.

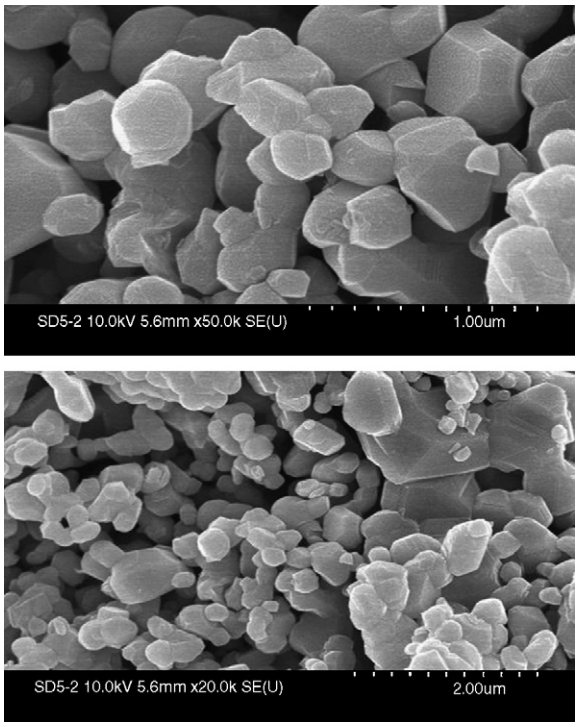

Fig. 2. SEM images of $Li[Li_{2/10}Ni_{1/10}Co_{2/10}Mn_{5/10}]O_2$.

3. Results and discussion

3.1. XRD and SEM characterization

Typical powder X-ray diffraction pattern recorded for the compound, $Li[Li_{2/10}Ni_{1/10}Co_{2/10}Mn_{5/10}]O_2$ is shown in Fig. 1. The XRD patterns are indexed in α-$NaFeO_2$ type structure, space group $R\bar{3}m$. The main peak, at $2\theta = 21°$–$25°$ appears as a result of short-range ordering of Li, Ni, Co, and Mn atoms in the transition metal layers [11,12]. The peaks at $2\theta = 45°$, 37°, 38°, 38.5°, 54.5° and 65.5° corresponding to the planes (1 0 4), (1 0 1), (0 0 6), (0 1 2), (0 1 8) and (1 1 0) respectively, substantiates the formation of hexagonal structure [23]. The lattice parameter, *a*, was calculated by Rietveld program (Fullprof 2000, LLB) as 2.844 Å. The significantly split (0 0 6), (1 0 2) and (1 0 8), (1 1 0) peak pairs in the XRD patterns and the *c*/*a* ratio, 4.99, indicate the formation of a layered structure. The integrated intensity ratio '*R*' of the (0 0 3) to (1 0 4) line was found to be 2.75. As pointed out by Dahn et al. [24] and Morales et al.

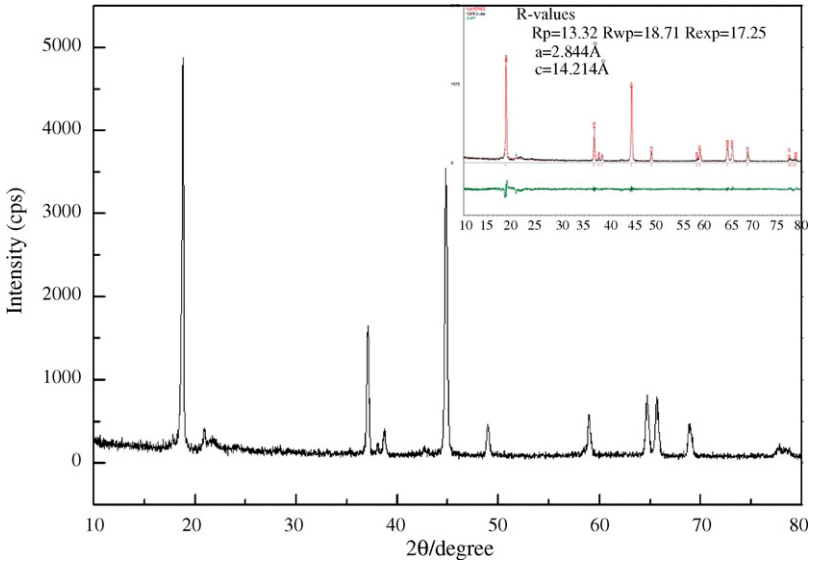

Fig. 1. Powder X-ray diffractogram of $Li[Li_{2/10}Ni_{1/10}Co_{2/10}Mn_{5/10}]O_2$.

[25] the higher intensity for the (0 0 3) reflection compared to the (1 0 4) reflection further confirms the formation of expected two-dimensional structure.

Fig. 2(a) and (b) depict the SEM pictures of the prepared compound $Li[Li_{2/10}Ni_{1/10}Co_{2/10}Mn_{5/10}]O_2$. The particles are more or less uniformly sized and seem to be hexagonally shaped and the average particle size of compound is 250–400 nm.

3.2. Differential capacity

The differential capacity plots were recorded between 2.5–4.1, 2.5–4.3, 2.5–4.5, 2.5–4.6 and 2.5–4.8 V for the sample $Li[Li_{2/10}Ni_{1/10}Co_{2/10}Mn_{5/10}]O_2$ and are displayed in Fig. 3(a)–(e), respectively, as this study is a complimentary and useful technique to evaluate the electrochemical characteristics of oxide cathode materials. As can be seen in the figures, there are two regions of electrochemical activity: one around 4.0 V, and the other one above 4.4 V. In the present study, in addition to the nickel ion other substituent, Co is also present. In addition to the electrochemical processes of Ni and Mn the properties of Co is also reflected. Fig. 3(a) shows the CV recorded between 2.5 and 4.1 V. The first anodic scan shows a broad peak around 3.9 V and a corresponding cathodic peak at the same potential. After that any discernible shifts could not be seen in the subsequent cycles and this electrochemical activity is attributed to $Co^{4+/3+}$ couple, which is responsible for major reduction and oxidation processes at 3.6–3.9 V [26]. The cyclic voltammogram (CV) of the cell between 2.5 and 4.3 V does not change much (Fig. 3(b)). More interestingly, on the other hand, the CV shows three distinct redox processes when cycled between 2.5 and 4.5 V (Fig. 3(c)). The first cycle shows anodic peaks at 3.3, 3.96 and 4.5 V and their corresponding cathodic peaks at 3.25, 3.8 and 4.4 V, respectively. But on the second cycle, the first anodic peaks are shifted to 3.2, 3.8 and 4.4 V and their corresponding cathodic peaks to 3.1, 3.75 and 4.3 V, respectively, which indicate better reversibility of the electrode [16]. A similar trend was observed when the cells were cycled between 2.5 and 4.6 V and 2.5–4.8 V. An apparent change was observed when the upper cut-off voltage of the cells was increased above 4.3 V. A new peak appears at 4.49, 4.48 and 4.55 in the Fig. 3(c)–(e), respectively, and abruptly disappears in the subsequent cycles. This new peak arises during the first charge process, when lithium is extracted from $Li[Li_{2/10}Ni_{1/10}Co_{2/10}Mn_{5/10}]O_2$ as-prepared sample and is attributed to irreversible capacity and this is reflected in the corresponding charge–discharge curves also (to be discussed in the next section). According to Lu and Dahn [11] and Park and Sun [12] this peak arises due to the removal of electrons from the oxygen atom in the structure of the cathode material at higher applied voltage which, results a partial loss of oxygen from the electrode. The observed peaks at 3.7 and 4.1 V in the first charge process are attributed to the oxidation of Ni^{2+} to Ni^{4+} in the material. On the other hand no oxidation peak of Mn^{3+} to Mn^{4+} could be observed in the first charging process, which, partially proves that the prepared pristine sample contains Mn^{4+} and is not involved in

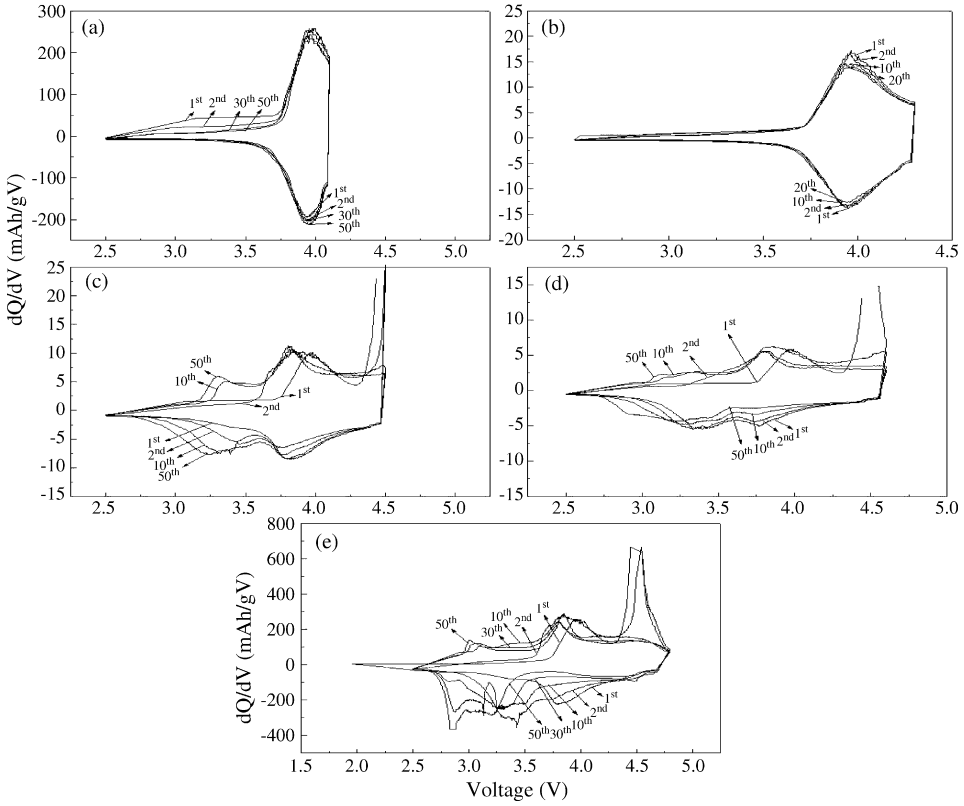

Fig. 3. Differential capacity vs. voltage plots of $Li[Li_{2/10}Ni_{1/10}Co_{2/10}Mn_{5/10}]O_2$/Li cells at different cell voltage regions: (a) 2.5–4.1 V; (b) 2.5–4.3 V; (c) 2.5–4.5 V; (d) 2.5–4.6 V; (e) 2.5–4.8 V.

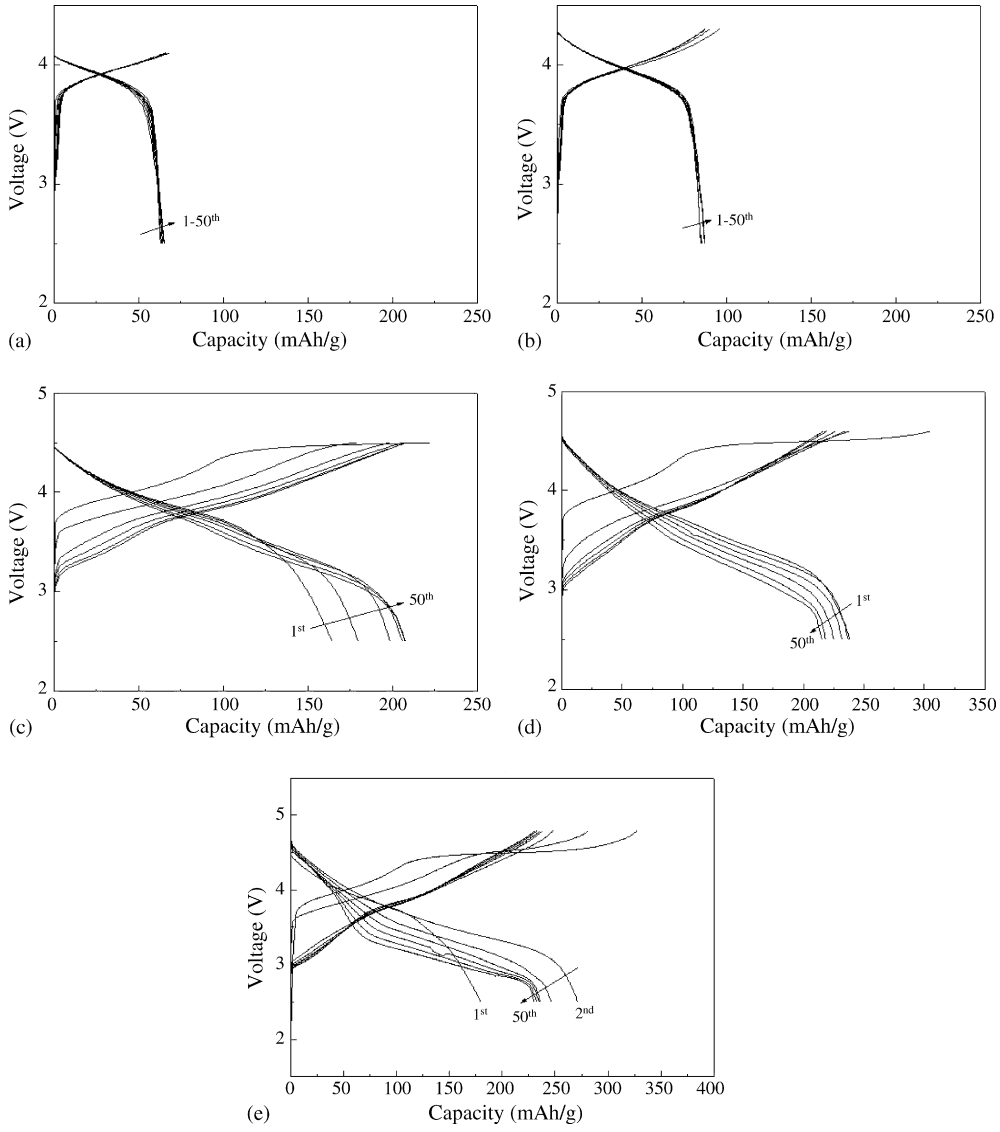

Fig. 4. A typical charge–discharge curve of the $Li[Li_{2/10}Ni_{1/10}Co_{2/10}Mn_{5/10}]O_2$/Li cells for different upper cut-off voltages: (a) 2.5–4.1 V; (b) 2.5–4.3 V; (c) 2.5–4.5 V; (d) 2.5–4.6 V; (e) 2.5–4.8 V.

the redox process. These results are in accordance with those reported earlier [11,12]. A discontinuity is seen at 4.4 V in all the cases and a similar behavior was obtained by Kim et al. [15] for the system $xLiNi_{1/2}Mn_{1/2}O_2(1-x)Li_2TiO_3$ and Shaju et al. [16] for $LiNi_{1/3}Co_{1/3}Mn_{1/3}O_2$. This is attributed to the intense charge transfer process during first oxidation and reduction process [16]. The oxidation and reduction process of $Mn^{4+/3+}$ is taking place at higher voltage region. According to Delmas et al. [27], the oxidation of Ni^{2+} is taking place very easily when compared to Mn^{3+} because in the layered oxides in which both Ni and Mn ions are present, the Ni^{2+} ($r_{Ni^{2+}} = 0.69$ Å) which, is bigger than that of Mn^{4+} ($r_{Mn^{4+}} = 0.53$ Å) or Mn^{3+} ($r_{Mn^{3+}} = 0.654$ Å) and the NiO_6 octahedra is more compressed than MnO_6 octahedra structure [28,29]. As discussed by Shaju et al. [16], the Mn^{3+} and Ni^{4+} are not clearly seen in the cyclic voltammetry and these ions are merged with that of Ni^{2+} and Ni^{4+} couple.

3.3. Charge–discharge studies

Electrochemical charge–discharge studies were performed in a galvanostatic mode between 2.5 to 4.8 V at 0.2 C rate. Typical charge–discharge profiles for all the voltage ranges are shown in Fig. 4(a)–(e). On starting the current, the voltage of the cell was suddenly increased to 3.75 V and then slowly increased to 4.1 V (Fig. 4(a)). These results are in accordance with those reported earlier [13,14,18]. Reflecting the cyclic voltammogram, the charge–discharge curves also showed a voltage plateau, the 3.7–3.9 V region. This compound showed an irreversible capacity loss about 10 mAh g^{-1} during the first charge–discharge cycle and there after shows a stable cycling. A similar observation was observed when the cells were cycled between 2.5 and 4.3 V (Fig. 4(b)) regions.

In order to gain the maximum possible capacity, the cells were cycled between 2.5–4.5, 2.5–4.6 and 2.5–4.8 V and

Table 1
The values of discharge capacities (DC) at the end of different cycles for different voltage ranges

Voltage range (V)	DC 1st cycle	DC 10th cycle	DC 20th cycle	DC 30th cycle	DC 40th cycle	DC 50th cycle
2.5–4.1	63.0	64.8	65.1	65.2	65.2	65.0
2.5–4.3	85.3	87.1	87.1	87.3	87.2	87.4
2.5–4.5	189.9	224.0	228.6	228.9	229	229
2.5–4.6	238.5	225.2	218.7	215.3	–	–
2.5–4.8	274.3	246.4	236.4	234.7	232.6	230.4

their corresponding discharge capacities are displayed in Fig. 4(c)–(e), respectively. Upon increasing the voltage, the length of the 4.5 V plateau is increased. It is seen in the figure that the initial discharge capacity of the system is 165 mAh g^{-1} with an irreversible capacity loss of about 60 mAh g^{-1} during first charge and discharge cycle. Further more when the voltage was increased to 4.6 and 4.8 their corresponding irreversible capacity has also been increased to 120 and 150 mAh g^{-1}, respectively. A similar observation has been reported by Shaju et al. [16] where the authors discussed the electrochemical properties and decomposition of electrolytes in the $Li[Mn_{0.5}Ni_{0.5}]O_2$ systems. Table 1 summarizes the discharge capacity of the $Li/Li[Li_{2/10}Ni_{1/10}Co_{2/10}Mn_{5/10}]O_2$ cells versus cycle number at different voltage regions. Voltage profile also mirrors the cyclic voltammetry data with two-voltage plateau system and an increase in the length of the 4.5 V plateau observed. According to Amine et al. [26] who reported the two-electron redox couple involving the transition of $Ni^{2+} \rightarrow Ni^{3+} \rightarrow Ni^{4+}$ based on XPS analysis that the minor amount of Mn^{3+} is responsible for this activity. The observed irreversible capacity loss of 60 mAh g^{-1} reveals full re-insertion of the extracted Li-ion is possible and is attributed to the cation mixing (Ni^{2+} occupy Li^+ site and vice-versa) in the compound. The sizes of the lithium ion (ionic radii $r_{Li^+} = 0.76$ Å and $r_{Li^{2+}} = 0.69$ Å) also facilitate for this event and subsequently collapse the inter slab space which results due to the oxidation of Ni^{2+} to Ni^{3+} or (Ni^{4+}). This eventually, leads to considerable irreversible capacity loss. The observed capacity fading in $Li[Li_{2/10}Ni_{1/10}Co_{2/10}Mn_{5/10}]O_2$ compound upon cycling could be due to the polarization of electrode and in addition to the decomposition of the electrolyte [16].

The discharge capacity of the $Li[Li_{2/10}Ni_{1/10}Co_{2/10}Mn_{5/10}]O_2/Li$ cells as a function of cycle number for various upper-cut off voltages are shown in Fig. 5. It can be seen from the figures that the discharge capacity of the cell $Li[Li_{2/10}Ni_{1/10}Co_{2/10}Mn_{5/10}]O_2/Li$ decreases exponentially up to 15 cycles then it becomes stable up to 50 cycles with a fade in capacity of 0.9 mAh g^{-1} when the upper cut-off voltage was 4.8 V. The theoretical capacity of the cathode material in the 5 V region was calculated as 307.02 mAh g^{-1}. A similar trend was observed when the upper cut-off voltage was 4.6 V. The observed increase of discharge capacity with the increase of upper cut-off voltage is attributed to the involvement of oxidation of Mn^{4+} to Mn^{5+} [30–33]. According to Sigala et al. [30] this plateau could be related to Mn^{5+}/Mn^{4+} couple or the removal of lithium. Hong et al. [34] also suggested that the oxidation of Mn^{4+} to Mn^{5+} is a unique property because it involves a change in the electronic configuration from d^3 to d^2. Some reports are also available on

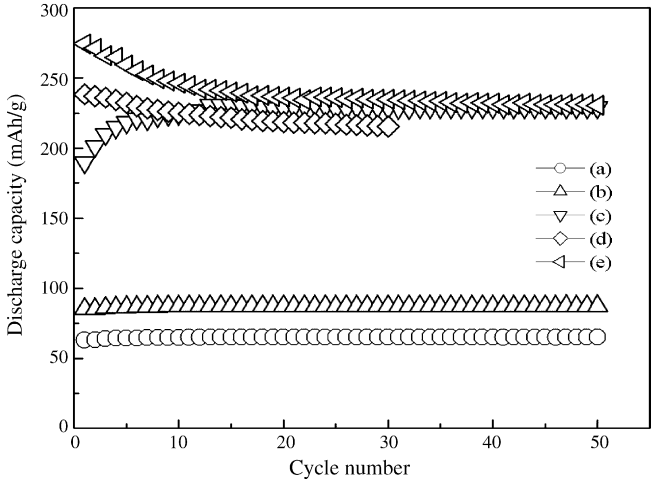

Fig. 5. Discharge capacity as a function of cycle number for the $Li[Li_{2/10}Ni_{1/10}Co_{2/10}Mn_{5/10}]O_2/Li$ cells: (a) 2.5–4.1 V; (b) 2.5–4.3 V; (c) 2.5–4.5 V; (d) 2.5–4.6 V; (e)2.5–4.8 V.

the redox activities of Mn in the 5 V region [35–37]. Further more the discharge capacity was increased (Fig. 5(c)) with the increase of cycle number (from 180 to 225 mAh g^{-1}) initially and becomes stable up to 50 cycles studied. This increase of discharge capacity at the initial stage is attributed to stabilization of manganese oxide structure upon cycling [38]. However, it is worthy to note when the cells were cycled between 2.5 and 4.5V the cycling stability was better at the expense of obtainable reversible capacity.

4. Conclusions

The layered compound $Li[Li_{2/10}Ni_{1/10}Co_{2/10}Mn_{5/10}]O_2$ was synthesized by sol–gel method with glycolic acid as chelating agent. The prepared compound was subjected to XRD and SEM analysis. The electrochemical profile of the compound was analyzed by CV and charge–discharge studies. Maximum irreversible capacity loss was observed in the 2.5–4.8 V region upon reducing the upper cut-off voltage to 4.2 V the cycling stability was better at the expense of obtainable reversible capacity.

Acknowledgement

This work was supported by Ministry of Science and Technology, 2004.

References

[1] Y. Xia, Y. Zhou, M. Yoshio, J. Electrochem. Soc. 144 (1997) 2593.
[2] A. Yamada, J. Solid State Chem. 122 (1996) 160.
[3] R.J. Gummow, C.N. Schmutz, A. Blyr, C. Singala, A.S. Gozdz, D. Larcher, J.M. Tarascon, J. Power Sources 69 (1997) 11.
[4] M.M. Thackeray, Prog. Solid State Chem. 25 (1997) 1.
[5] R. Alcantara, J. Morales, J.L. Tirado, E. Zhecheva, R. Stoyanova, J. Electrochem. Soc. 142 (1995) 3997.
[6] R. Alcantara, J. Morales, J.L. Tirado, E. Zhecheva, R. Stoyanova, Ionics 1 (1995) 246.
[7] S.A. Campell, C. Bows, R.S. McMillan, J. Electroanal. Chem. 284 (1990) 195.
[8] A. Manuel Stephan, Dale-Teeters, Electrochim. Acta 45 (2003).
[9] T. Ohzuku, A. Ariyoshi, S. Takeda, Y. Sakai, Electrochim. Acta 46 (2001) 2327.
[10] D.H. Sang, S.M. Oh, J. Electrochem. Soc. 144 (1997) 3342.
[11] Z. Lu, J.R. Dahn, J. Electrochem. Soc. 149 (2002) A815.
[12] S.H. Park, Y.K. Sun, J. Power Sources 119–121 (2003) 161.
[13] T. Ohzuku, Y. Makimura, Chem. Lett. (2001) 744.
[14] Z. Lu, L.Y. Beaulieu, R.A. Donaberger, C.L. Thomas, J.R. Dahn, J. Electrochem. Soc. 149 (2002) A778.
[15] J.S. Kim, J.S. Johnson, M.M. Thackeray, Electrochem. Commun. 4 (2002) 205.
[16] K.M. Shaju, G.V. Subba Rao, B.V.R. Chowdari, Electrochim. Acta 48 (2002) 145.
[17] Z. Jiang, K.M. Abraham, J. Electrochem. Soc. 143 (1996) 1591.
[18] J.M. Tarascon, W.R. Mckinoon, F. Coowar, T.N. Bowmer, G. Amatucci, D. Guyomard, J. Electrochem. Soc. 141 (1994) 1421.
[19] V. Manev, W. Ebner, W. Thompson, S. Dow, US Patent 5,961,949 (1999).
[20] M.M. Thackeray, P.G. Johnson, L.A. Picciotto, P.G. Bruce, J.B. Goodenough, Mater. Res. Bull. 19 (1984) 179.
[21] Y. Gao, J.R. Dahn, J. Electrochem. Soc. 143 (1996) 100.
[22] T. Tsumura, A. Shimizu, M. Inagaki, J. Mater. Chem. 3 (1993) 995.
[23] K.S. Park, M.H. Choe, S.J. Jin, K.S. Nahm, Y.S. Hong, Solid State Ionics 171 (2004) 141.
[24] J.R. Dahn, U. von Sacken, C.A. Michael, Solid State Ionics 44 (1990) 87.
[25] J. Morales, C. Perez-Vicente, J.L. Tirado, Mater. Res. Bull. 25 (1990) 623.
[26] K. Amine, H. Yukamoto, H. Yasuda, Y. Fujita, J. Power Sources 68 (1997) 604.
[27] C. Delmas, M. Menetrier, L. Croguennec, S. Levasseur, J.P. Peres, C. Pouillerie, G. Prado, L. Fournes, F. Weill, Int. J. Inorg. Mater. 1 (1999) 11.
[28] R.D. Shannon, Acta Crystallogr. Sect. A 32 (1976) 751.
[29] A.R. Armstrong, A.D. Robertson, R. Gitzendanner, P.G. Bruce, J. Solid State Chem. 145 (1999) 549.
[30] C. Sigala, A. Veraere, J.L. Mansot, D. Guyomard, Y. Piffard, M. Tournoux, J. Solid State Chem. 132 (1997) 372.
[31] S.H. Hong, S.H. Chang, C.H. Yo, Bull. Korean Chem. Soc. 20 (1999) 372.
[32] J.B. Bates, D. Lubben, N.J. Dudney, F.X. Hart, J. Electrochem. Soc. 142 (1995) L149.
[33] G.T.K. Fey, C.Z. Lu, T. Prem Kumar, Mater. Chem. Phys. 80 (2003) 309.
[34] S.H. Hong, S.H. Chang, C.H. Yo, Bull. Korean Chem. Soc. 20 (1999) 53.
[35] Y. Shao Horn, R.L. Middaugh, Solid State Ionics 139 (2001) 13.
[36] G.T.K. Fey, C.Z. Lu, T. Prem kumar, J. Power Sources 115 (2003) 332.
[37] Y.I. Jiang, B. Huang, W. Wang, D.R. Sadoway, G. Ceder, Y.M. Chiang, H. Liu, H. Tamura, J. Electrochem. Soc. 146 (1999) 862.
[38] K.S. Park, M.H. Cho, S.J. Jin, K.S. Nahm, Electrochem. Solid State. Lett. 7 (2004) A239.